

Mesomorphic– α -Monoclinic Phase Transition in Isotactic Polypropylene: A Study of Processing Effects on Structure and Mechanical Properties

Sara A. Arvidson,[†] Saad A. Khan,^{*†} and Russell E. Gorga^{*‡}

[†]*Department of Chemical and Biomolecular Engineering and* [‡]*Department of Textile Engineering, Chemistry and Science, North Carolina State University, Raleigh, North Carolina 27695*

Received January 21, 2010; Revised Manuscript Received February 18, 2010

ABSTRACT: We report the enthalpy for the mesomorphic to α -monoclinic phase transition in polypropylene under varying thermal treatments. The mesomorphic phase is created by fiber spinning and rapid quenching methods and identified using wide-angle X-ray diffraction and differential scanning calorimetry. Fiber mesomorphs are found to have a 3-fold increase in enthalpy of transition per gram of mesophase compared with our measurements of quenched polypropylene and previous reports of quenched polypropylene. In addition, systematic tensile testing over a range of spin speeds and polymer morphologies reveals that the presence of mesomorphic regions does not correlate with reduced fiber strength as has been previously suggested. Fiber true stress–true strain curves obtained at varying take-up velocities are compared to determine the “tensile strain shift”, which should theoretically provide a measure of molecular orientation. We find that the tensile strain shift correlates with birefringence, thereby providing an alternative method to assess molecular orientation in fibers, an important factor for fiber strength. This approach can prove useful for fibers in which measuring the molecular orientation via birefringence is not an option.

1. Introduction

Much work has been done to produce fibers by and model high-speed melt spinning¹ for the production of high-tenacity filaments for a number of polymers.^{2–6} Such processes generally include postspinning drawing steps that result in greater molecular orientation in the fiber. Though similar in many ways to melt spinning, nonwovens processes that aim to create high-strength webs from fibers in a single continuous process such as spunbonding⁷ or melt blowing may present extra challenges due to their coupled spin-draw step. While both melt spinning and nonwovens processes were commercialized by the 1950s,⁸ a much greater emphasis on modeling in the literature has been applied to generalized melt-spun fiber formation and use.

Because of relative ease of spinning, low cost, and rapid crystallization, isotactic polypropylene (iPP) is one of the most commonly spun polymers in nonwovens processes. iPP crystallization is a complex process that involves several crystalline morphologies and competing crystallization mechanisms that depend greatly on temperature and stress. iPP has been shown to crystallize predominately in the α -monoclinic form under isothermal crystallization,⁹ in slow cooling,¹⁰ and during melt spinning of filaments.¹¹ The β -hexagonal or γ -triclinic polymorphs may be obtained while crystallizing from the melt at high undercoolings or pressures or with the addition of nucleating agents.^{12–16} The “meso” polymorph, often described as a smectic or paracrystalline phase, has been identified in iPP treated by very high rates of cooling from the melt,^{17,18} isothermal crystallization between 0 and 40 °C,¹⁹ and in fiber spinning at moderate take-up velocities, high extrusion temperatures, low molecular weight distributions, and low draw-down ratios.^{11,12,20–22} The mesomorph is not an imperfect crystal, but rather has molecular ordering between that of the amorphous phase and a true crystalline

phase;²³ mesomorphic iPP has a high degree of order in the direction of the chain axis but little in its lateral packing.²⁴ Mesomorphs are not unique to iPP, having been shown for a wide variety of polymers including polyesters and polysiloxanes,²⁵ and are important for improving polymer clarity²⁶ and possibly polymer processability.²⁴

Both the α and meso iPP polymorphs are composed of 3₁ helices. While the arrangement of the left- and right-handed helices of the mesomorphic form are disordered, left and right helices follow a well-defined sequence of handedness in the α form.^{27,28} Upon heating, the meso phase transforms into the α phase, possibly by thickening of existing α crystals and/or by structural rearrangements in the mesomorphic phase.²⁹ The mechanism of this structural rearrangement has yet to be determined in any conclusive way.^{18,28,30–33} Androsch²⁸ observed the meso-to- α phase transition through atomic force microscopy of nanoscale domains and determined that initial mesomorphic domains were not destroyed during the phase transformation but could not rule out local melting within domains. Consequently, it is unclear if the meso-to- α phase transition occurs via melting into the liquid state or rather by a direct solid-to-solid transition. Two possible mechanisms of the meso-to- α transition have been discussed, one involving chains unwinding to reverse handedness and the other requiring chain translocation without changing handedness.^{28,33}

Extensive work has been published describing the effect of spinning conditions on the development of orientation in the α , β , and amorphous phases in iPP fibers, yet orientation development of the mesophase (and the mesophase in general) has largely been ignored in fibers.²¹ While orientation of the amorphous phase has been linked to fiber strength,³⁴ with crystallites acting as network junctions,³⁵ the role of mesophases on mechanical properties is ambiguous. It has been suggested that mesophase content poses significant detriment to the strength of iPP fibers³⁶ and increases ductility in quenched films,³⁷ yet polymer mesophases are credited with improving mechanical properties and processability

*Corresponding authors: e-mail russell_gorga@ncsu.edu, Ph 919-515-6553 (R.E.G.); e-mail khan@eos.ncsu.edu, Ph 919-515-4519 (S.A.K.).

Table 1. Physical Properties of iPP Resins

resin	iPP _S (Sunoco)	iPP _E (Exxon)
MW _n (Da)	58500 ^a	
MW _w (Da)	160000 ^c	153000 ^c
PDI	3.04, ^a 3.24 ^c	3.51 ^c
melt flow rate (MFR) (dg min ⁻¹)	35, ^a 35 ^c	35, ^a 37 ^c
zero shear viscosity (Pa s)	682 ^b	747 ^b
isotacticity <i>mmmm</i> (by NMR)	0.95 ^a	
isotacticity <i>mmmm</i> (by FTIR)	0.93 ^b	0.94 ^b

^aReported by manufacturer. ^bMeasured by the authors. ^cCorrelated to dynamic rheological properties.

over crystalline phases.²⁴ Further gains in defining structure–property relationships for semicrystalline polymers have not been made due to an incomplete understanding of viscoelastic and viscoplastic responses of the various morphologies present in the polymer, during the melt solidification stage or during mechanical tests at ambient temperature.³⁸ An overwhelming majority of studies on the thermal behavior of iPP surrounding the meso-to- α transition focuses on mesomorphic iPP formed by rapid quenching rather than fiber spinning. Estimated enthalpies of the meso-to- α phase transition range from 8.8 to 16.7 J g⁻¹ for quench-formed meso iPP due to varying polymer thermal histories, experimental methodologies, and polymer grades,^{30,39–41} which makes accurately determining the meso and crystalline content of iPP materials by differential scanning calorimetry (DSC) difficult. Additionally, it has been shown that the enthalpy of the meso-to- α phase transition may differ for fibers and quench-formed meso iPP.³⁶

In this study we compare the enthalpy of the iPP meso-to- α phase transition of fibers to that of quenched polymer and discuss the implications of the enthalpy in terms of supporting existing theories of the mechanism of this phase transition. Further, we report the mechanical properties and orientation functions of meso-containing iPP fibers in the context of melt spinning and spunbonding routes of iPP fiber formation and assess the dependence of the mesomorphic phase orientation on take-up velocity with a three-phase model. We begin with a discussion of fibers containing mesophase iPP and follow with that of quenched-formed iPP, ultimately comparing the thermal properties of each.

2. Experimental Section

2.1. Materials and Sample Processing. Commercially available iPP formulations with similar molecular weight profiles were selected from two manufacturers: iPP_S (Sunoco Chemicals Polymers Division, product CP360H) and iPP_E (ExxonMobil Chemical, product PP3155) (Table 1). Melt-spun iPP_S and iPP_E fibers were produced at the Hills spinning line in the College of Textiles Fiber Science Lab at NC State University at take-up velocities up to 2000 m min⁻¹. No secondary drawing was applied to melt-spun fibers. Spunbond iPP_S fibers were produced at the Nonwovens Cooperative Research Center (NCRC) Partners' Pilot facilities located at NC State over a range of aspirator pressures. Fibers were collected following extrusion but before the bonding step so that the as-spun morphology could be studied. All fibers were spun with mass throughputs of 0.4 g hole⁻¹ min⁻¹. Fibers were also collected for each process without the use of the godet or aspirator pressure with the intent of creating unoriented, isotropic fibers at a low take-up velocity. This velocity (≈ 20 m min⁻¹) is referred to as the “free fall” velocity. The densities of semicrystalline fibers were estimated from the densities for 100% crystalline, amorphous, and mesomorphic iPP: $\rho_C = 0.936$, $\rho_A = 0.858$, and $\rho_M = 0.916$ g cm⁻³.^{42,43} Because of the nature of spunbonding, individual fiber take-up velocities are variable and unknown at the time of formation. The equivalent take-up velocities for spunbond fibers are calculated from the continuity equation (eq 1) to facilitate comparison between spunbond fibers and melt-spun fibers, for which take-up velocity V (m min⁻¹) is

directly controlled.

$$V = \frac{Q}{\rho A_c} \quad (1)$$

In eq 1, Q is the throughput (g hole⁻¹ min⁻¹), ρ is the polymer density (g m⁻³), and A_c is the average cross-sectional area of an individual fiber (m²).

Quenched iPP_S and iPP_E polymers were prepared by heating the respective resins in a furnace to 225 °C until molten (~ 5 min), pressing the molten polymer between sheets of aluminum, and holding in a furnace at 225 °C for 15 min. Samples were removed from the furnace directly into a quench bath. iPP_E was quenched in ice–water (0 °C), while iPP_S was quenched at four different conditions: ice–water (0 °C), acetone–dry ice (-78 °C), pentane–liquid N₂ (-131 °C), and liquid N₂ (-196 °C).^{41,44} Quenched polymers were then brought up to, stored, and indexed at room temperature.

2.2. DSC Measurements. The crystalline (x_C), mesomorphic (x_M), and amorphous (x_A) fractional content was determined using a TA Instruments Q2000 model differential scanning calorimeter. Scans were carried out on 6 to 12 mg samples in standard aluminum pans calibrated to an indium standard. Heating rates, unless otherwise specified, were 10 °C min⁻¹ under 50 mL min⁻¹ N₂ purge. To identify the fraction of polymer in the crystalline phase, the heat of fusion for a sample ΔH_m was compared to the heat of fusion of a gram of 100% crystalline polypropylene ΔH_m^0 according to eq 2.

$$x_C = \frac{\Delta H_m}{\Delta H_m^0} \quad (2)$$

$\Delta H_m^0 = 207$ J g⁻¹ was used for 100% crystalline iPP.⁴⁵

2.3. Wide-Angle X-ray Diffraction (WAXD) Measurements. X-ray diffraction studies were conducted with a Cu K α radiation source ($\lambda = 1.542$ Å) at 40 kV \times 30 mA for 1800 s on a Bruker D-5000 diffractometer equipped with a Highstar area detector. Diffraction patterns were analyzed with Bruker General Area Detector Diffraction System (GADDS) software. Fibers were aligned by winding around a frame and placed in the apparatus oriented vertically, with the plane of the fibers perpendicular to the X-ray beam. In transmission mode, the intensity was recorded for 2θ in the range of 10°–32°. Scans taken with an empty sample holder served as a background for subtraction. Orientation of the crystalline regions with respect to the fiber axis can be determined according to the method of Wilchinsky assuming rotational symmetry about the fiber axis, as shown in eq 3, and by employing the Hermans–Stein orientation factor, eq 4.^{46–48}

$$\cos^2 \phi_{j,z} = \frac{\int_0^{\pi/2} I_{hkl}(\phi_{j,z}) \cos^2(\phi_{j,z}) \sin \phi_{j,z} d\phi_{j,z}}{\int_0^{\pi/2} I_{hkl}(\phi_{j,z}) \sin \phi_{j,z} d\phi_{j,z}} \quad (3)$$

$$f_j = \frac{3 \cos^2(\phi_{j,z}) - 1}{2} \quad (4)$$

Here, I_{hkl} is the intensity diffracted from the (hkl) planes which are normal to the j -crystallographic axis. In α -monoclinic iPP, the helices lay along the c -crystallographic axis, which lacks a convenient reflection, so the intensities of the $\langle 110 \rangle$ and $\langle 040 \rangle$ bands were integrated as a function of the azimuthal angle. The average cosine squared of the angle between the fiber axis and the c -axis can be calculated according to eq 5.

$$\cos^2 \phi_{c,z} = 1 - 1.1099 \cos^2(\phi_{110,z}) - 0.901 \cos^2 \phi_{040,z} \quad (5)$$

Mesomorphic iPP was modeled as a hexagonal crystal.⁴⁹ Because of symmetries within a hexagonal crystal,⁵⁰ only one

reflection is required to characterize the mesomorphic orientation, which was estimated according to eq 6.

$$\cos \phi^2_{c,z} = 1 - 2 \cos^2(\phi_{0002,z}) \quad (6)$$

2.4. Fiber Mechanical Testing. Mechanical testing of fibers was conducted on an Instron model 5544 at ambient conditions and analyzed with Bluehill v. 1.00 software. The Instron was fitted with 0.9 cm clamps and a 5 N load cell. Single filaments with a gage length of 28.6 mm were drawn at a crosshead speed of 25.4 mm/min until breakage occurred.

2.5. Microscopy. Fiber diameters measured by optical microscopy were used to calculate fiber cross-sectional areas. The refractive indices of polypropylene fibers were measured by a Mach–Zehnder type interference microscope by Aus Jena with polarized green light ($\lambda = 546$ nm). Fiber birefringence (Δn) was calculated from refractive indices (n) in the directions parallel and normal to the fiber axis.

$$n_{\parallel \text{ or } \perp} = n_o + \frac{Z\lambda}{DB} \quad (7)$$

$$\Delta n = n_{\parallel} - n_{\perp} \quad (8)$$

Here, Z is the width of fringes, B is the fringe shift, and n_o is the refractive index of the immersion oil.

Birefringence relates to the molecular orientations of each phase according to

$$\Delta n = x_C f_C \Delta_C^o + x_A f_A \Delta_A^o + x_M f_M \Delta_M^o \quad (9)$$

where we have included the mesomorphic phase contributions to the total birefringence. Intrinsic birefringences (Δ^o) used were 0.331, 0.040, and 0.0468 for the crystalline, mesomorphic, and amorphous iPP phases, respectively.^{34,43,51,52} Calculation of the orientation functions of the crystalline and mesomorphic phases (f_C and f_M) are described by eq 4 while eq 9 is used to solve for the amorphous orientation function (f_A). Equation 9 ignores the form birefringence which takes into account the crystallite shape and generally only contributes 5–10% of the overall birefringence for most polymers. However, polypropylene has been reported to have negligible form birefringence.³⁴

3. Results and Discussion

3.1. Fiber Extrusion: Morphology and Molecular Orientation. Figure 1 shows WAXD spectra for iPP_S spunbond, iPP_S melt-spun, and iPP_E melt-spun fibers for a range of take-up velocities. WAXD patterns exhibiting strong peaks located at $2\theta = 14.2^\circ$, 17.1° , and 18.7° correspond to the (110), (040), and (130) α -monoclinic reflections, respectively,^{53,54} while broad reflections at $2\theta = 15^\circ$ and 21° correspond to mesomorphic iPP.⁵⁵ Melt-spun and spunbond fibers exhibit α reflections at both low and high take-up velocities. Because of the ease of controlling the take-up velocity on a melt spinning line, fibers were obtained at very low to moderate velocities ($20 < V < 1600$ m min⁻¹) that were not always possible with the spunbond process. However, where similar take-up velocities were obtained by both processes, melt-spun and spunbond fibers possessed similar crystalline morphology (in Figure 1: compare A with B and D with E).

Focusing first on lower speeds, WAXD patterns for iPP_S melt-spun fibers are dominated by mesomorphic reflections for take-up velocities at or above about 100 m min⁻¹ up to about 1000 m min⁻¹. iPP_E, however, contained a mixture of α and meso phases at the lowest possible V (free fall extrusion, ≈ 20 m min⁻¹), and crystallization was completely suppressed in favor of meso formation at velocities as low as 30 m min⁻¹.

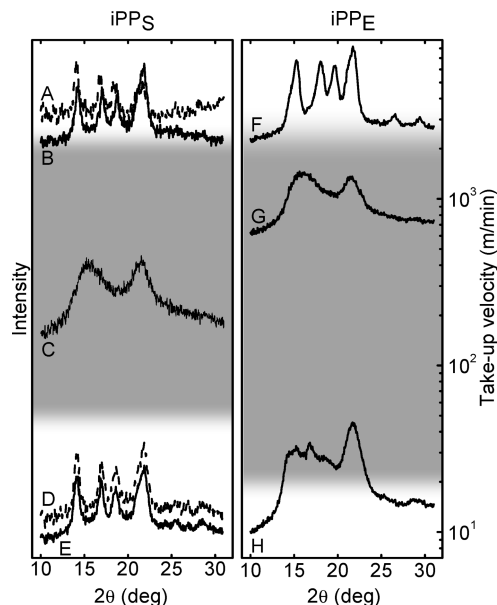


Figure 1. WAXD spectra for isotactic polypropylene (iPP) fibers. Subscripts “S” and “E” refer to source of polymer, S corresponding to Sunoco and E to Exxon. (A) Spunbond iPP_S, 2000 m min⁻¹. (B) Melt-spun iPP_S, 2000 m min⁻¹. (C) Melt-spun iPP_S, 300 m min⁻¹. (D) Spunbond iPP_S, ≈ 20 m min⁻¹. (E) Melt-spun iPP_S, ≈ 20 m min⁻¹. (F) Melt-spun iPP_E, 2000 m min⁻¹. (G) Melt-spun iPP_E, 1000 m min⁻¹. (H) Melt-spun iPP_S, ≈ 20 m min⁻¹. Shaded areas indicate approximate spin speeds resulting in mesomorphic formation.

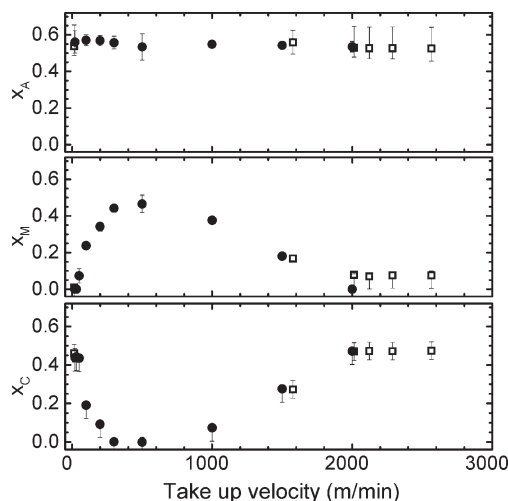


Figure 2. Mass fraction of each phase for iPP_S fibers determined by DSC. Subscripts refer to amorphous (A), mesomorphic (M), and crystalline (C) phases. Fibers with filled symbols were prepared by melt spinning and open symbols by spunbonding.

Both iPP_S and iPP_E redeveloped α -crystallinity above about 1500 m min⁻¹. Annealing the mesophase at 120 °C, which is below the melting point of iPP, results in replacement of mesomorphic phase with α -monoclinic phase (for figure, see Supporting Information). Figure 2 summarizes the as-spun phase composition as determined by DSC of melt-spun and spunbond iPP_S fibers, which are consistent with WAXD results. The mesomorphic fraction was determined using the enthalpy of the meso-to- α phase transition for a given sample relative to the enthalpy required to convert a sample of 100% mesophase to the α -form; the details of establishing the reference enthalpy in fibers (43.7 J g_{meso}⁻¹) are the subject of section 3.4. Note that the amorphous content of fibers is essentially constant over the entire range of take-up

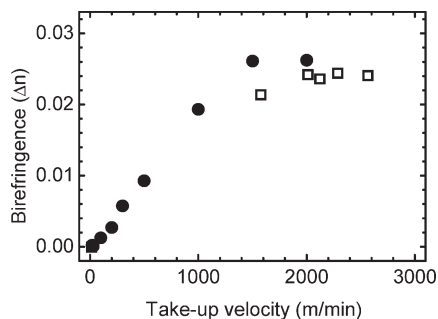


Figure 3. Birefringence versus take up velocity for iPP_S fibers. Fibers with filled symbols were prepared by melt spinning and open symbols by spunbonding.

velocities at 55%; the total of the mesomorphic and crystalline phases are limited to and compete for the remaining 45% of the polymer mass in the fibers. Therefore, as the as-spun fraction of mesomorph changes with take-up velocity, the crystalline content responds with an equal and opposite change, which can be seen in the plots of meso and crystalline fractions that are mirror images of each other with respect to take-up velocity (Figure 2).

Fiber birefringence, which indicates the overall molecular orientation,⁵⁶ is reported in Figure 3. Fibers produced at the free fall velocity ($\approx 20 \text{ m min}^{-1}$) were unoriented on a molecular scale. The overall orientation increased monotonically with take-up velocity but remained constant above 1500–2000 m min^{-1} for melt-spun fibers. Spunbond fibers followed a similar trend, reaching maximum Δn between 1600 and 2000 m min^{-1} . Bosley⁵⁶ discussed fiber molecular orientation in terms of fiber length, where the length of an as-spun fiber is related to the theoretical length that fiber would have if the orientation could be relaxed to zero. Similarly, as an unoriented fiber is subjected to macroscopic deformation in the form of tensile extension, the molecular orientation increases along with length. In theory for semicrystalline polymers, isotropic fibers should contain the entire stress–strain profile (“master curve”) for the polymer, where the true strain can be thought of as the length of the fiber as it is drawn. Figure 4A shows the true stress (σ_T) versus true strain (ϵ_T) for melt-spun and spunbond fibers at a range of take-up velocities (and hence as-spun molecular orientations). By superimposing each of the curves onto the master curve via shifting them along the strain axis (Figure 4B), it can be seen that as take-up velocity increases, each curve begins at an incrementally higher strain or “length”. The percent strain required to overlay a curve to the master curve is referred to here as the strain shift ($\Delta\epsilon_T$). There were no significant differences between the strain shift calculated for spunbond and melt-spun fibers produced at equivalent take-up velocities. Figure 5 shows Δn versus $\Delta\epsilon_T$ for the series of spunbond and melt-spun fibers. For Δn above about 0.003, $\Delta n \sim \Delta\epsilon_T$. However, at lower orientations, the strain shift is more sensitive to increases in take-up velocity (and possibly orientation) than Δn . At orientations relevant to fiber formation, the strain shift may be an excellent and convenient predictor of overall molecular orientation and fiber strength, both of which are discussed in further detail below.

The overall molecular orientation reflects the sum of the orientations in the amorphous, crystalline, and, in the case of iPP , mesomorphic phases (eq 9). Figure 6 shows the orientation functions for each phase as a function of melt-spun or spunbond take-up velocity. Crystalline orientation increased with take-up velocity up to a maximum but did not change with further increasing take-up velocity. Amorphous

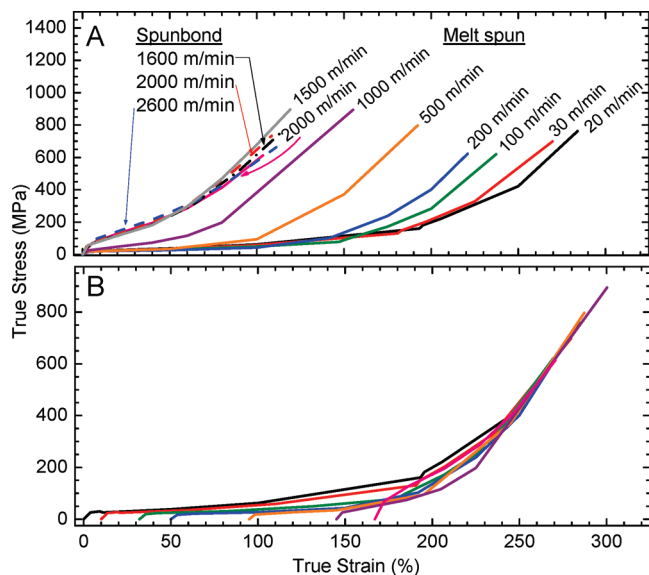


Figure 4. (A) True stress versus true strain for melt-spun (solid) and spunbond (dashed) iPP_S single filaments at ambient conditions. Curves are averages of 8–10 samples. (B) Data from above with curves shifted horizontally to create a master curve.

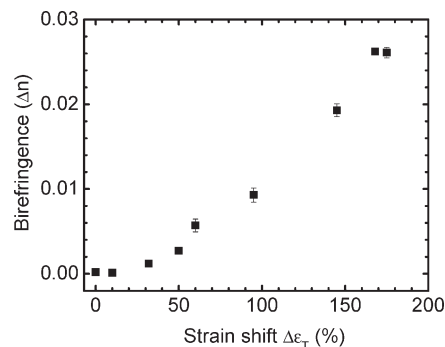


Figure 5. Birefringence versus true strain shift ($\Delta\epsilon_T$, from Figure 4B) for iPP_S fibers.

orientations of both the spunbond and melt-spun fibers increased sharply with increasing take-up velocity up to $\approx 2000 \text{ m min}^{-1}$ but did not change with further increase in take-up velocity. Comparing Figure 6B with Figure 3, the amorphous orientation appears to scale approximately with Δn . From this, we estimate that for spunbonding or other fiber-forming processes that do not utilize postspinning draw steps, it may be possible to relate iPP amorphous orientation to birefringence and hence to strain shift. Perhaps more importantly, one may gain insight into the as-spun amorphous phase and its solidification during fiber extrusion by a single, straightforward tensile test such as the strain shift procedure shown here.

Because the mesomorphic phase is not considered a true crystalline phase, there are no established methods for quantifying meso orientation using WAXD. However, realizing that WAXD detects long-range ordering in the direction of the PP chain axis in the mesomorphic phase (Figure 1) and that the meso and α phases compete for the same *nonamorphous* 45% of the polymer’s mass (Figure 2), we consider the meso phase pseudocrystalline for the purpose of measuring its orientation by WAXD. For melt-spun fibers produced from 200 to 1000 m min^{-1} , the absence of strong α reflections (Figure 1) allowed us to quantify the mesomorphic orientation function. Figure 6C

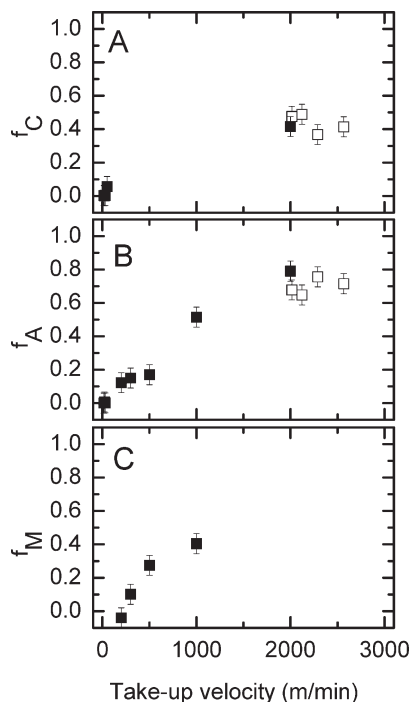


Figure 6. Orientation function versus take-up velocity for the (A) crystalline, (B) amorphous, and (C) mesomorphic phase calculated for iPP_S fibers. Fibers with filled symbols were prepared by melt spinning and open symbols by spunbonding.

shows that at low velocities (e.g., 200 m min⁻¹) the meso phase of iPP has random orientation ($f_M \approx 0$). With increasing take-up velocity, the average angle between the fiber axis and the mesophase regions decreases (hence, $f_M > 0$); this indicates that the mesophase orients preferentially in the direction of the fiber long axis with increasing take-up velocity in a manner similar to the amorphous and crystalline regions. The α phase prevents significant meso formation at take-up velocities above about 1600 m min⁻¹. We were not able to deconvolute the XRD reflections as a function of azimuthal angle for melt-spun fibers produced at 100 and 1500 m min⁻¹ or spunbond fibers produced at 1577 m min⁻¹ where significant fractions of both α and meso phases coexist and overlap in both the 2θ and azimuthal directions.

In practice, calculating the amorphous orientation requires knowledge of the intrinsic birefringences of each phase of the polymer. Intrinsic birefringences can be calculated if the phase content of the material and the orientation of each phase are known for a series of samples, which means that the amorphous orientation must be calculated from another independent set of measurements such as the sonic modulus or FTIR analysis. While this appears rather straightforward, a series of four experimental measurements are required for each sample in the series (density, birefringence, X-ray diffraction, and sonic modulus), so the calculated intrinsic birefringences are very sensitive to experimental error. It is not surprising, therefore, that several values have been reported in the literature,^{34,51,52} the median of which was used to calculate the orientation functions in this work. While we believe the trends are accurate and the orientations realistic, we provide the caveat that the calculated orientations presented here depend greatly on the value of the intrinsic birefringence one chooses to employ.

The strain shift reflects various degrees of molecular deformation and can be used to evaluate the mechanisms

of deformation.⁵¹ Affine deformations involve network junctions separated by flexible chains, where junctions are displaced in proportion to the amount of deformation as the polymer is stretched. This type of deformation can be modeled according to eq 10, where $\langle P2 \rangle$ is an orientation parameter which we take to represent the overall or individual phase orientation functions, the fitting parameter N represents the number of chain segments between network points, Δn_{\max} is the maximum birefringence for a polymer, and $\Delta \varepsilon_T$ can be related to the network draw ratio (ω) according to eq 11.⁵⁷⁻⁵⁹

$$\langle P2 \rangle = \frac{\Delta n}{\Delta n_{\max}} = \frac{1}{5N} \left(\omega^2 - \frac{1}{\omega} \right) \quad (10)$$

$$\omega = \frac{\Delta \varepsilon_T}{100\%} + 1 \quad (11)$$

Pseudoaffine deformations do not involve extension of individual elements, but rather rigid segments that rotate in proportion to macroscopic deformations, which can be modeled according to eq 12.

$$\begin{aligned} \langle P2 \rangle &= \frac{\Delta n}{\Delta n_{\max}} \\ &= \frac{1}{2} \left(\frac{2\omega^3 + 1}{\omega^3 - 1} - \frac{3\omega^3}{(\omega^3 - 1)^{3/2}} \arctan((\omega^3 - 1)^{1/2}) \right) \end{aligned} \quad (12)$$

Figure 7A shows that macroscopically (that is, in terms of overall orientation) iPP fibers are consistent with affine deformation. Several values for the fitting parameter N are shown; $N = 1.46, 2.00,$ and 1.49 correspond to the least squared difference for the region where $\omega < 2, \omega > 2,$ and for the entire range of ω , respectively. The affine model well-describes the amorphous phase (Figure 7B), while the pseudoaffine model qualitatively predicts the *shape* (convex down) of the meso phase curve (Figure 7C), though it does not allow for the meso formation and orientation only at $V \geq 100$ m min⁻¹. The crystalline phase orientation (not shown) cannot be definitively fitted to either the affine or pseudoaffine deformation mechanisms due to the absence of crystallinity at intermediate orientations (see Figure 2). This indicates that deformation mechanisms can be evaluated using the strain shift in the amorphous and mesomorphic phases for iPP. Further, because the amorphous phase is shown to follow affine-type response when the *nonamorphous* fraction is mesomorphic, crystalline, or a combination of both, the data would suggest that the mesomorphic and crystalline regions can both act as “network junctions” connected by amorphous “flexible chains”.

The mechanical properties of mesomorphic-containing fibers have not been studied in a comprehensive manner, though Nitta and Odaka⁶⁰ found that the Young’s modulus of iPP meso phase is between that of the amorphous and crystalline phases and that the yield strength of the meso phase is lower than that of crystalline iPP.⁶⁰ Both of these findings would suggest that the mesophase mechanical properties are intermediate to the amorphous and crystalline phases and support the use of a three-phase model (such as eq 9) to account for mesomorphic contributions to a measurable quantity, which are distinct from amorphous and crystalline contributions. Figure 4 shows that fibers containing

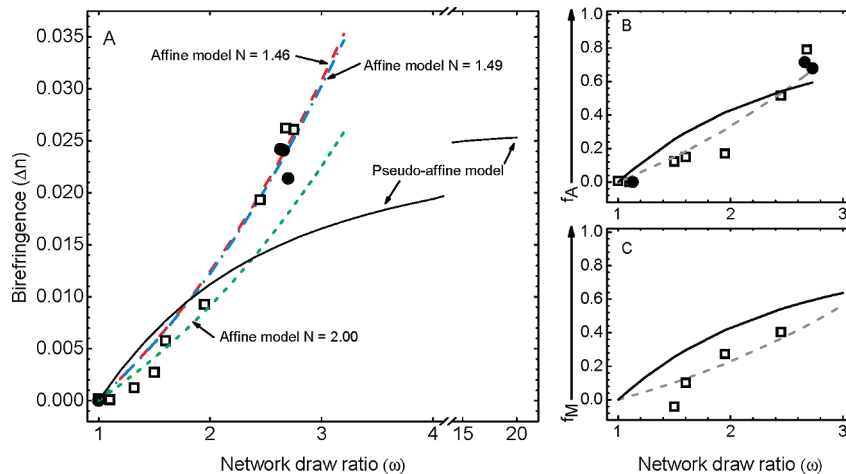


Figure 7. (A) Birefringence, (B) amorphous orientation function, and (C) mesomorphic orientation function versus network draw ratio for PP spunbond (●) and melt-spun (□) fibers. Predictions based on affine (dashed lines, with varying fitting parameter N) and pseudoaffine models (solid lines).

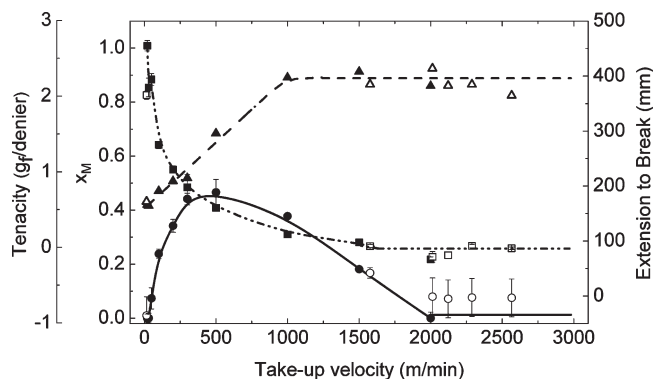


Figure 8. Tenacity (triangles, large dash), extension to break (squares, small dash), and mass fraction mesomorphic phase (circles, solid) versus spin speed for melt-spun (filled symbols) and spunbond (unfilled symbols) fibers. Error bars indicate standard error and trend lines are to guide the eye.

even large percentages of mesomorphic iPP (200–1000 min^{-1}) fit the true stress–true strain master curve and together Figures 4 and 5 show that over the take-up velocity series the strain shift increases monotonically over changing morphologies and most clearly relates to increases in orientation, regardless of crystalline morphology. Most convincingly, Figure 8 shows two measures of fiber strength, tenacity, and elongation to break, plotted with the fraction of mesomorphic material present in iPP_S fibers. If the mesomorphic phase were harmful to fiber strength, we would expect the tenacity to be highest at very low and high spin speeds where no meso phase was present. By visual inspection, the tenacity appears to be dependent on orientation instead (compare Figures 3 and 8). Taken together, we conclude that the mesomorphic phase does not deleteriously affect iPP fiber strength (compare to a recent study³⁶ which did not address fiber size or control for fiber molecular orientation between mesomorphic and α -crystalline iPP fibers).

3.2. Polymer Quenching: Morphology. Next, the thermal properties of mesomorphic iPP created by two distinct sets of thermal treatment conditions are compared: (1) applied stress and cooling that occurs during fiber spinning and (2) rapid quenching in the absence of applied stress. Mesomorphic morphology resulted from quenching iPP_E in

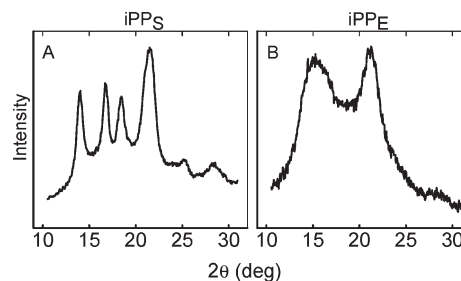


Figure 9. WAXD spectra for (A) iPP_S, liquid N₂ quenched, and (B) iPP_E, quenched in ice–water.

conditions as mild as ice-water (0 °C). However, we were unable to form discernible fractions of mesomorphic phase for iPP_S in even with our harshest quenching conditions (liquid nitrogen) (Figure 9), despite the ability of the iPP_S resin to form the mesomorph during fiber spinning (compare with Figure 1C).

3.3. Resin Properties: iPP_S and iPP_E. Because of subtle differences in polymer architectures or formulations, the mesomorphic form was easier to develop in iPP_E than iPP_S; the iPP_E meso phase occurred at the lowest possible take-up velocity and under mild quench, while iPP_S required take up velocities of at least 100 m min^{-1} and presumably quench rates much greater than we were able to achieve with a liquid N₂ quench bath. Isotacticity is thought to play an important role in mesomorphic formation. The isotacticities of iPP_S and iPP_E are reported in Table 1. Relatively low isotacticity in PP ($m\text{mmmm} < 0.89$) has led to meso phase in fiber extrusion at moderate velocities, while highly isotactic PP ($m\text{mmmm} > 0.97$) gave strictly α -crystalline fibers at all velocities,²¹ which is in good agreement with what we found for both resins (mesomorphic phase present at moderate take-up velocities for $m\text{mmmm} \approx 0.93\text{--}0.95$). However, the inability to suppress crystallization by rapid quenching of iPP_S was surprising; iPP_S isotacticity is well above the predicted minimum critical requirement to produce meso phase ($m\text{mmmm} \geq 0.680$)²³ and is similar to the iPP_E isotacticity. In addition, both resins possess similar melt flow indices, zero shear viscosities, and transitions from Newtonian to shear thinning behavior (i.e., viscosity dependence on shear rate; data included as Supporting Information) as well as molecular weights (MW) and polydispersities (PDI)

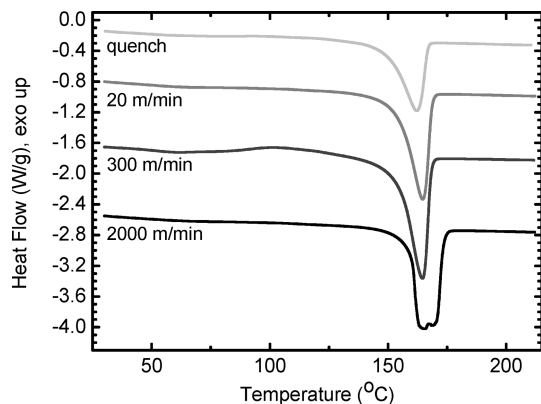


Figure 10. DSC heating thermograms of quench cooled iPP_E and iPP_S fibers with a heating rate of $10\text{ }^\circ\text{C min}^{-1}$.

(Table 1). Therefore, the inability to form mesophase at the same conditions in the two resins are attributed to differences in resin production which could include residual catalyst or other materials which nucleate crystallization in the iPP_S formulation.

3.4. Thermal Processing and Mesomorphic Formation.

Figure 10 shows the heat flow versus temperature for selected melt-spun fibers and quenched polymer. Fibers produced by melt spinning or spunbonding exhibit a single or double, broad melting endotherm depending on take-up velocity. At moderate take-up velocities (e.g., 300 m min^{-1}), DSC traces also exhibit a small, wide exotherm at $\approx 100\text{ }^\circ\text{C}$, indicative of the mesomorphic to α phase transition.⁶¹ The appearance of this exotherm corresponds with the appearance of mesomorphic reflections by WAXD (compare Figures 1 and 10). When the mesomorph is present, determining x_C or x_M in a fiber by DSC is difficult; ignoring the meso exotherm results in an overestimate of the crystallinity of an as-spun fiber, yet reported values for $\Delta H_{M\rightarrow\alpha}$ are based on quench studies of the iPP meso phase, not fiber extrusion, which makes any estimate of the mesomorphic mass fraction dubious. Therefore, we investigated the enthalpy of the meso-to- α phase transition as a function of polymer processing. We assume that melt-spun fibers produced at 300 and 500 m min^{-1} contained no measurable α -crystalline fraction based on both WAXD and DSC and (refer to Figures 1 and 10) and that crystalline material produced during the course of the DSC heating ramp occurred via the mesomorphic-to- α route only.^{31,33} We integrated the heating curves to obtain the exotherm associated with the meso-to- α transition ($\Delta H'_{M\rightarrow\alpha}$, $\text{J g}_{\text{sample}}^{-1}$) and the endotherm associated with the melting of the transformed crystals (ΔH_m , $\text{J g}_{\text{sample}}^{-1}$). Comparing ΔH_m to ΔH_m^0 according to eq 2, we were able to calculate the fraction crystallinity in the samples which resulted from transforming the mesomorphic phase (x_C') which is identical to the fraction mesomorphic phase present in the unheated sample (x_M). The enthalpy associated with the meso-to- α transition ($\Delta H_{M\rightarrow\alpha}$, $\text{J g}_{\text{meso}}^{-1}$) was calculated by dividing $\Delta H'_{M\rightarrow\alpha}$ by x_M according to eq 10.

$$\Delta H_{M\rightarrow\alpha} = \frac{\Delta H'_{M\rightarrow\alpha}}{x_M} \quad (10)$$

Once $\Delta H_{M\rightarrow\alpha}$ had been determined from samples containing no crystalline material before heating, the mesomorphic content of samples with both mesomorphic and crystalline fractions can be evaluated by comparing $\Delta H'_{M\rightarrow\alpha}$ to $\Delta H_{M\rightarrow\alpha}$ in a manner similar to calculating the crystallinity by comparing a melting endotherm to the standard melting

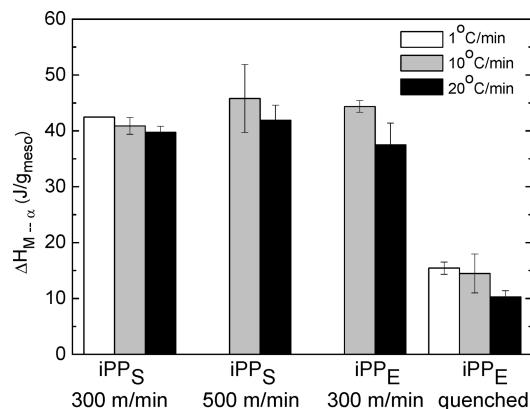


Figure 11. Enthalpy of the mesomorphic-to- α phase transition in iPP fibers and quenched polymer for heating rates of 1 – $20\text{ }^\circ\text{C min}^{-1}$.

endotherm. By reporting the specific enthalpy $\Delta H_{M\rightarrow\alpha}$ rather than the observed enthalpy $\Delta H'_{M\rightarrow\alpha}$, we hope to determine unambiguously the enthalpy of this phase transition that is specific to fiber formation and which can be applied to fibers with varying x_M .

$\Delta H_{M\rightarrow\alpha}$ for quenched iPP_E ($14.5\text{ J g}_{\text{meso}}^{-1}$, Figure 11) agrees well with those values reported for other quenched iPP resins. The melt-spun fiber iPP_E $\Delta H_{M\rightarrow\alpha}$, however, is more than 3 times greater ($\sim 43.7\text{ J g}_{\text{meso}}^{-1}$, Figure 11). While thermal processing clearly affects $\Delta H_{M\rightarrow\alpha}$, the heat measured for this phase transition is independent of the polymer (iPP_S compared to iPP_E) and the rate of heating over the range of 1 – $20\text{ }^\circ\text{C min}^{-1}$. The amorphous fraction remaining in the quenched polymer is much higher (0.67) than for fibers (0.55), which suggests that during quenching the polymer was cooled more rapidly than in fiber spinning and/or that the molecular orientation that results during fiber spinning aids in the formation of the mesomorphic phase. The wide range of values for the enthalpy of phase transition reported in the literature may be due to varying, yet unaccounted for, x_M resulting from varied rates of quench. Note that x_M of fibers, calculated using DSC and reported in Figure 2, were determined using the enthalpy of phase transition determined in this work of $43.7\text{ J g}_{\text{meso}}^{-1}$.

3.5. Mechanism of Meso-to- α Phase Transition. Two potential mechanisms, reversing helix handedness and chain motion (translation) while retaining handedness, have been provided to explain the mesomorphic-to- α phase transition.^{28,33} Reversing handedness for poly(β -phenylpropyl L-aspartate)⁶² and polytetrafluoroethylene⁶³ has been shown, as well as the enthalpy associated with uncoiling carrageenan double helices.⁶⁴ However, reversing of handedness is considered to be an unlikely molecular event for polyolefins.⁶⁵ Instead, helical phase II to helical phase I transitions in *i*-poly(1-butene) result from translation, not changes in handedness. Multiple, competing mechanisms of phase transformation have been shown for poly(*N*-isopropylacrylamide), where the enthalpy of phase change depends on whether the polymer undergoes mostly intrachain folding or interchain aggregation, which is dictated by heat treatments or solution conditions.⁶⁶ The magnitude of the differences in $\Delta H_{M\rightarrow\alpha}$ in iPP for each thermal treatment (i.e., fiber extrusion compared to quenching) indicates that fiber spinning creates a more thermally stable mesophase than quenching. The existence of distinct $\Delta H_{M\rightarrow\alpha}$ for quenching and fiber extrusion may support the theory of multiple available mechanisms for the meso-to- α phase transition, where each can act simultaneously depending on the thermal treatment of the polymer.

4. Conclusions

The enthalpy of the meso-to- α phase transition in iPP has been reported for quenched iPP and fibers spun from iPP. The enthalpy of phase transition for quenched polymer is in agreement with previous reports, while the fiber enthalpy of phase transition was much greater, indicating a more thermally stable phase in spun fibers. Therefore, the $\Delta H_{M \rightarrow \alpha}$ for the quenched polymer does not accurately predict the crystallinity in fibers. Orientation of the mesomorphic phase was estimated using traditional crystal orientation theory for X-ray diffraction and resulted in realistic orientations similar to those of true crystalline phases. Molecular orientation of all three phases (crystalline, mesomorphic, and amorphous) increased with increasing take-up velocity to a point. Mechanical properties of iPP showed no correlation to the presence of the mesomorphic phase but clearly related to molecular orientation. Tensile strain was shown to predict molecular orientation for iPP fibers, where the strain shift was linearly proportional to the overall molecular orientation in the fibers for a wide range of orientations. This suggests that strain shift can be used as an effective alternate approach to assessing molecular orientation in fibers and may prove particularly valuable for fibrous systems where birefringence cannot be used.

Acknowledgment. The authors gratefully acknowledge the Nonwovens Cooperative Research Center (NCRC) for financial support of this work. Thanks are also due to Dr. Mehdi Afshari, Ms. Birgit Andersen, and Ms. Michelle Casper for their analytical assistance, Drs. Jon-Paul Maria and Eunyoung Shim for the use of their laboratories, and Drs. Behnam Pourdeyhimi, Jan Genzer, Carol Hall, and Alan Tonelli for fruitful discussions.

Supporting Information Available: WAXD patterns of melt-spun iPP_S: as-spun (300 m min⁻¹) having mesomorphic structure and annealed at 120 °C having α -monoclinic structure; zero-shear viscosity of iPP_E and iPP_S. This material is available free of charge via the Internet at <http://pubs.acs.org>.

References and Notes

- Melt spinning is a method of producing extruded, spun filaments that are collected onto a winder. Once collected, filaments can be woven into textiles or randomized to form a nonwoven material.
- Kim, K. H.; Cho, H. H.; Ito, H.; Kikutani, T. *J. Polym. Sci., Part B: Polym. Phys.* **2008**, *46*, 847–856.
- Buckley, C. A.; Lautenschlager, E. P.; Gilbert, J. L. *J. Appl. Polym. Sci.* **1992**, *44*, 1321–1330.
- Mezghani, K.; Spruiell, J. E. *J. Polym. Sci., Part B: Polym. Phys.* **1998**, *36*, 1005–1012.
- Hahm, W. G.; Ito, H.; Kikutani, T. *Int. Polym. Proc.* **2006**, *21*, 536–543.
- Bhuvanesh, Y. C.; Gupta, V. B. *J. Appl. Polym. Sci.* **1995**, *58*, 663–674.
- Spunbonding is a method of producing nonwovens by depositing extruded, spun filaments onto a collection belt. Filaments are randomized onto the collection belt by air jets, which create a web that is subsequently bonded using heated rolls. In this study, melt-spun and spunbond processes differ in the method of controlling fiber take-up velocity: melt-spun fibers utilize a winder while spunbonding employs air jets to draw fibers. Using air jets in spunbonding has the consequence of changing the cooling rate of the molten polymer.
- McCulloch, J. *Int. Nonwovens J.* **1999**, *8*, 139–149.
- Kim, Y. C.; Ahn, W.; Kim, C. Y. *Polym. Eng. Sci.* **1997**, *37*, 1003–1011.
- Natta, G. *J. Polym. Sci.* **1955**, *16*, 143–154.
- Lengyel, M.; Mathe, K.; Bodor, G. *Acta Chim. Acad. Sci. Hung.* **1977**, *94*, 309–320.
- Broda, J. *J. Appl. Polym. Sci.* **2003**, *89*, 3364–3370.
- Kardos, J. L.; Christia, Aw; Baer, E. *J. Polym. Sci., Part A-2: Polym. Phys.* **1966**, *4*, 777–&.
- Libster, D.; Aserin, A.; Garti, N. *Polym. Adv. Technol.* **2007**, *18*, 685–695.
- Romankiewicz, A.; Sterzynski, T.; Brostow, W. *Polym. Int.* **2004**, *53*, 2086–2091.
- Varga, J.; Ehrenstein, G. W. *Polymer* **1996**, *37*, 5959–5963.
- Gailey, J. A.; Ralston, R. H. *SPE Trans.* **1964**, *4*, 29–33.
- Hanna, L. A.; Hendra, P. J.; Maddams, W.; Willis, H. A.; Zichy, V.; Cudby, M. E. A. *Polymer* **1988**, *29*, 1843–1847.
- De Santis, F.; Adamovsky, S.; Titomanlio, G.; Schick, C. *Macromolecules* **2007**, *40*, 9026–9031.
- Zhang, X. Q.; Li, R. B.; Kong, L.; Wang, D. J. *Polymer* **2008**, *49*, 1350–1355.
- Choi, D. M.; White, J. L. *Polym. Eng. Sci.* **2004**, *44*, 210–222.
- Andreassen, E.; Grostad, K.; Myhre, O. J.; Braathen, M. D.; Hinrichsen, E. L.; Syre, A. M. V.; Lovgren, T. B. *J. Appl. Polym. Sci.* **1995**, *57*, 1075–1084.
- Konishi, T.; Nishida, K.; Kanaya, T.; Kaji, K. *Macromolecules* **2005**, *38*, 8749–8754.
- Auriemma, F.; De Rosa, C.; Corradini, P. Solid mesophases in semicrystalline polymers: Structural analysis by diffraction techniques. In *Interphases and Mesophases in Polymer Crystallization II*, 2005; Vol. 181, pp 1–74.
- Li, L. B.; de Jeu, W. H. Flow-induced mesophases in crystallizable polymers. In *Interphases and Mesophases in Polymer Crystallization II*, 2005; Vol. 181, pp 75–120.
- Lieberman, R.; Stewart, C. Polypropylene Polymers. *Encyclopedia of Polymer Science and Technology*; John Wiley & Sons: 2002; Vol. 11, pp 287–358.
- Miller, R. L. *Polymer* **1960**, *1*, 135–143.
- Androsch, R. *Macromolecules* **2008**, *41*, 533–535.
- Martorana, A.; Piccarolo, S.; Sapoundjjeva, D. *Macromol. Chem. Phys.* **1999**, *200*, 531–540.
- Fichera, A.; Zannetti, R. *Makromol. Chem., Macromol. Chem. Phys.* **1975**, *176*, 1885–1892.
- Konishi, T.; Nishida, K.; Kanaya, T. *Macromolecules* **2006**, *39*, 8035–8040.
- Zia, Q.; Androsch, R.; Radosch, H. J.; Piccarolo, S. *Polymer* **2006**, *47*, 8163–8172.
- Gomez, M. A.; Tanaka, H.; Tonelli, A. E. *Polymer* **1987**, *28*, 2227–2232.
- Samuels, R. J. *Structured Polymer Properties: The Identification, Interpretation, and Application of Crystalline Polymer Structure*; Wiley: New York, 1974.
- Drozdov, A. D. *Compos. Sci. Technol.* **2006**, *66*, 2648–2663.
- Cao, J. N.; Sbarski, I. *Polymer* **2006**, *47*, 27–31.
- Seguela, R.; Staniek, E.; Escaig, B.; Fillon, E. *J. Appl. Polym. Sci.* **1999**, *71*, 1873–1885.
- Drozdov, A. D.; Christiansen, J. D. *Comput. Mater. Sci.* **2007**, *39*, 729–751.
- Grebowicz, J.; Lau, S. F.; Wunderlich, B. *J. Polym. Sci., Polym. Symp.* **1984**, 19–37.
- O’Kane, W. J.; Young, R. J.; Ryan, A. J.; Bras, W.; Derbyshire, G. E.; Mant, G. R. *Polymer* **1994**, *35*, 1352–1358.
- Caldas, V.; Brown, G. R.; Nohr, R. S.; Macdonald, J. G.; Raboin, L. E. *Polymer* **1994**, *35*, 899–907.
- Zhang, D.; Bhat, G. J.; Sanjiv, M.; Wadsworth, L. *Text. Res. J.* **1998**, *68*, 27–35.
- Russo, R.; Vittoria, V. *J. Appl. Polym. Sci.* **1996**, *60*, 955–961.
- Gordon, A. J.; Ford, R. A. *The Chemist’s Companion*; Wiley: New York, 1972.
- Blaine, R. L. Thermal Applications Note. TN048 Polymer Heats of Fusion, TA Instruments, New Castle, DE.
- Wilchinsky, Z. W. *J. Appl. Phys.* **1960**, *31*, 1969–1972.
- Afshari, M.; Kotek, R.; Gupta, B. S.; Kish, M. H.; Dast, H. N. *J. Appl. Polym. Sci.* **2005**, *97*, 532–544.
- Nadella, H. P.; Henson, H. M.; Spruiell, J. E.; White, J. L. *J. Appl. Polym. Sci.* **1977**, *21*, 3003–3022.
- Compostella, M.; Bertinotti, F.; Coen, A. *Angew. Chem., Int. Ed.* **1962**, *74*, 618–&.
- Cullity, B. D. *Elements of X-ray Diffraction*, 2nd ed.; Addison-Wesley Publishing Co.: Reading, MA.
- Ward, I. M. *Structure and Properties of Oriented Polymers*, 2nd ed.; Chapman & Hall: New York, 1997.
- Masuko, T.; Tanaka, H.; Okajima, S. *J. Polym. Sci., Part A-2: Polym. Phys.* **1970**, *8*, 1565–&.
- Wang, X. Y.; Gong, R. H. *Macromol. Mater. Eng.* **2006**, *291*, 499–509.
- Lafrance, C. P.; Prudhomme, R. E. *Polymer* **1994**, *35*, 3927–3935.

- (55) Yan, R. J.; Li, W.; Li, G.; Jiang, B. Z. *J. Macromol. Sci., Phys.* **1993**, *B32*, 15–31.
- (56) Bosley, D. E. *J. Polym. Sci., Part C: Polym. Symp.* **1967**, 77–104.
- (57) Penning, J. P.; van Ruiten, J.; Brouwer, R.; Gabrielse, W. *Polymer* **2003**, *44*, 5869–5876.
- (58) Hamza, A. A.; Sokkar, T. Z. N.; El-Farahaty, K. A.; El-Dessouky, H. M. *Polym. Test.* **2004**, *23*, 203–208.
- (59) El-Dessouky, H. M.; Mahmoudi, M. R.; Lawrence, C. A.; Yassien, K. M.; Sokkar, T. Z. N.; Hamza, A. A. *Polym. Eng. Sci.* **2009**, *49*, 2116–2124.
- (60) Nitta, K.; Odaka, K. *Polymer* **2009**, *50*, 4080–4088.
- (61) Mileva, D.; Androsch, R.; Zhuravlev, E.; Schick, C. *Macromolecules* **2009**, *42*, 7275–7278.
- (62) Watanabe, J.; Okamoto, S.; Satoh, K.; Sakajiri, K.; Furuya, H.; Abe, A. *Macromolecules* **1996**, *29*, 7084–7088.
- (63) Kimmig, M.; Strobl, G.; Stuhn, B. *Macromolecules* **1994**, *27*, 2481–2495.
- (64) Grinberg, V. Y.; Burova, T. V.; Grinberg, N. V.; Usov, A. I.; Tur, D. R.; Papkov, V. S. *Polym. Sci., Ser. A* **2009**, *51*, 390–395.
- (65) Lotz, B.; Mathieu, C.; Thierry, A.; Lovinger, A. J.; De Rosa, C.; de Ballesteros, O. R.; Auriemma, F. *Macromolecules* **1998**, *31*, 9253–9257.
- (66) Ding, Y. W.; Zhang, G. Z. *Chin. Sci. Bull.* **2009**, *54*, 1908–1911.